B **43**, 2007 (1991); *Nature* **355**, 328 (1992).
2. S. Kitamura *et al.*, *Nature* **351**, 215 (1991).
3. R. M. Feenstra, A. J. Slavin, G. A. Held, M. A. Lutz, *Phys. Rev. Lett.* **66**, 3257 (1991).
4. Y.-W. Mo *et al.*, *ibid.*, p. 1998.
5. E. Ganz *et al.*, *ibid.* **68**, 1567 (1992).
6. J. J. Metois and G. Le Lay, *Surf. Sci.* **133**, 422 (1983).
7. R. S. Becker, J. A. Golovchenko, B. S. Swartzentruber, *Phys. Rev. Lett.* **54**, 2678 (1985); R. Feidenhans'l *et al.*, *Phys. Rev. B* **38**, 9715 (1988); R. S. Becker, B. S. Swartzentruber, J. S. Vickers, T. Klitsner, *ibid.* **39**, 1633 (1989); T. Klitsner and J. S. Nelson, *Phys. Rev. Lett.* **67**, 3800 (1991); R. M. Feenstra and A. J. Slavin, *Surf. Sci.* **251/252**, 401 (1991); J. J. Boland, *Science* **255**, 186 (1992).
8. C. Kittel, *Introduction to Solid State Physics* (Wiley, New York, 1976), p. 94.
9. This energy barrier is not exactly equal to the Pb-Ge bond energy. The barrier also depends on the configuration of surrounding adatoms and rest atom dangling bonds. Here we just want to get a crude estimate of the mean lifetime of substitutional Pb atoms on T_4 sites. Furthermore, this energy barrier should be less than 0.54 eV, the activation energy for Pb atom diffusion (*5*), for the diffusion involves breaking more than one Pb–Ge bond. Taking 0.54 eV as E_D in the Arrhenius equation, we get 0.17 ms (at room temperature), an upper bound for the mean lifetime. It is still much too fast for the scanning tip to resolve this motion.
10. A detailed discussion of the role of nearby domain walls, stacking faults, and point defects in enhancing or pinning the row shift needed to form this metastable structure will be given elsewhere (*11*).
11. I. S. Hwang, S. K. Theiss, J. Golovchenko, in preparation.
12. We acknowledge helpful discussion with E. Kaxiras, S. K. Theiss, R. Martinez, E. Ganz, and F. Spaepen. Supported by the Office of Naval Research, the Materials Research Laboratory at Harvard University, and the Joint Services Electronics Program.

27 May 1992; accepted 1 September 1992

Direct Mechanical Measurements of the Elasticity of Single DNA Molecules by Using Magnetic Beads

Steven B. Smith, Laura Finzi,* Carlos Bustamante†

Single DNA molecules were chemically attached by one end to a glass surface and by their other end to a magnetic bead. Equilibrium positions of the beads were observed in an optical microscope while the beads were acted on by known magnetic and hydrodynamic forces. Extension versus force curves were obtained for individual DNA molecules at three different salt concentrations with forces between 10^{-14} and 10^{-11} newtons. Deviations from the force curves predicted by the freely jointed chain model suggest that DNA has significant local curvature in solution. Ethidium bromide and 4′,6-diamidino-2-phenylindole had little effect on the elastic response of the molecules, but their extent of intercalation was directly measured. Conversely, the effect of bend-inducing *cis*-diamminedichloroplatinum (II) was large and supports the hypothesis of natural curvature in DNA.

The ability of DNA to pack and fold into chromosomes or to serve as a template during transcription and replication depends on the particular elastic properties of the molecule as modified by local interactions. Light scattering, sedimentation velocity, viscometry, electro-optics, and ligase-catalyzed cyclization have been used to characterize these properties, but these bulk methods have several limitations (*1*). First, the elastic parameters are not directly observed in these measurements and must be obtained through model-dependent theories. Second, these macroscopic measurements represent ensemble averages over all accessible molecular configurations, providing little information about unlikely, extended states of the molecule. Third, measurements are often restricted to a limited range of ionic strength, temperature, and other variables.

Real-time fluorescence microscopy of single DNA molecules in solution (*2*–*6*) suggests that it should be possible to determine directly the strain-stress relation of single DNA molecules (*7*). These mechanical measurements could: (i) reveal the molecular mechanisms responsible for the elastic response of the molecule over a full range of forces and extensions; (ii) provide a more strict test of theories of polymer elasticity with molecules of known composition and size over a broad range of experimental conditions; and (iii) help improve present theories of gel electrophoresis (*8*), linear dichroism (*9*), and charge density (*10*).

The freely jointed chain model (FJC) treats the polymer as a chain of statistically independent (Kuhn) segments of length b whose orientations are uncorrelated in the absence of external forces. A force F acting on the free end of a molecule whose other end is attached to a fixed point stretches the polymer as each segment tends to align with the force. The external force is opposed by the polymer because of thermal agitation, which tends to disorder the segments. In this model, the elastic response of the molecule is purely entropic, and the force-dependent end-to-end distance, $\langle x \rangle$, in terms of the molecular contour length (L), the temperature T, and the Boltzmann constant k_B is (*11*):

$$\langle x \rangle = L\left(\coth\frac{Fb}{k_BT} - \frac{k_BT}{Fb}\right) = L\,\mathcal{L}\left(\frac{Fb}{k_BT}\right) \quad (1)$$

The expression in brackets is the Langevin function ($\mathcal{L}$). This relation can be inverted to give:

$$F = \frac{k_BT}{b}\mathcal{L}^{-1}\left(\frac{\langle x \rangle}{L}\right) \quad (2)$$

This model accounts for the bending rigidity of the molecule in terms of the single parameter b. The stiffer the molecule, the longer the Kuhn segment. An alternative description, the worm-like chain (WLC) (*12*), uses persistence length as a measure of chain stiffness. In the absence of external forces the Kuhn segment corresponds to twice the persistence length of the molecule (*12*).

Individual multimers of λ-DNA (48.5 kbp) were chemically attached by one of their ends to a glass slide and by their other end to a magnetic bead (*13*). A cover slip was used to enclose the anchored molecules into a fluid microchamber that fits on a microscope stage (Fig. 1A). The tethered beads were subjected to various combinations of magnetic and hydrodynamic forces applied along perpendicular directions by using movable magnets and variable flows (Fig. 1A). Arbitrarily large forces could be applied with flow, but their magnitude was difficult to determine directly because flow shear next to the glass surfaces made fluid velocity difficult to estimate there. Conversely, magnetic forces are typically not greater than 1 piconewton (pN) but can be made arbitrarily small and are easier to measure (see below). Flow forces could then be calibrated against the measured magnetic forces.

During an experiment, each combination of magnetic and hydrodynamic force displaced the bead and extended the molecule along a particular angle θ relative to the direction of the magnetic force (Fig. 1B). The greater the flow, the larger the angle with the horizontal axis. As opposite directions of the magnetic and flow forces were combined, the bead positions described a characteristic "ellipse" (Fig. 1B). Positions were observed on a television monitor and recorded by means of a computer cursor (*14*). From these data, the extension of the molecule from its point of attachment to the glass and the relative magnitudes of the magnetic and hydrodynamic forces were obtained.

Four ethidium-stained λ-dimers tether-

Institute of Molecular Biology and Department of Chemistry, University of Oregon, Eugene, OR 97403.

*Present address: Biochemistry Department, Brandeis University, Waltham, MA 02254.
†To whom correspondence should be addressed.

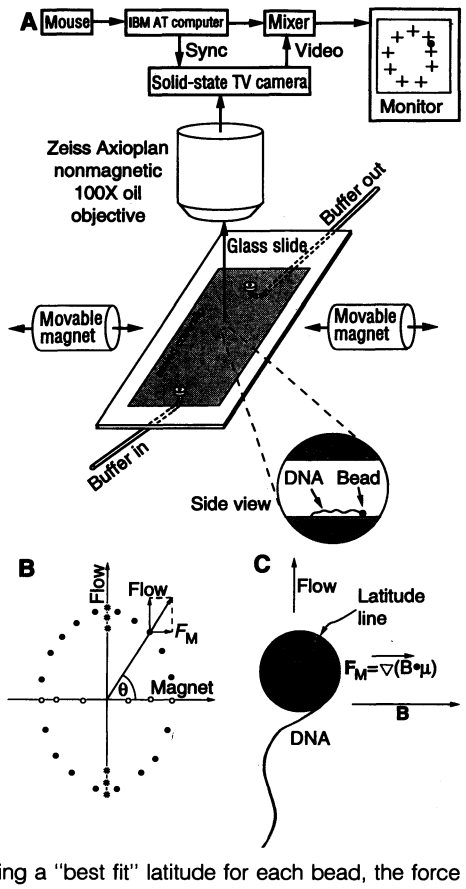

Fig. 1. (**A**) Microchamber made from glass slide and cover slip. Nd-Fe-B magnets (1-cm diameter) were moved to repeatable positions as close as 9 mm from the objective's center. Buffer flow was maintained by a constant pressure system. A computer cursor superimposed on the microscope image was used to record the equilibrium bead positions, time-averaged over their Brownian motion. Video and optical distortions were canceled by a computer mapping program calibrated against an objective micrometer. The magnetic bead was tethered by a DNA molecule (*12*). (**B**) Ellipse of bead positions obtained from various combinations of flow and magnetic forces. Magnetic forces were determined by Stokes' law for all magnet positions. The strongest magnet force is F_M. (●) High-force positions with the strongest magnetic force and various flows. The flow force is $F_M\tan(\theta)$, and the total force stretching the DNA along angle θ is $F_M\sec(\theta)$. (*) Positions with zero magnetic force and high flow forces as determined previously with magnets and holding flow constant. (○) Low-force positions at zero flow and weak magnetic forces. (**C**) The extension of the DNA is the shortest path from its point of attachment on the bead to that on the glass. Each bead is internally anisotropic, giving it a permanent magnetic dipole μ, which very nearly aligns with the external magnetic field **B**. The bead attachment point is constrained to some arbitrary latitude line, with the bead free to rotate about μ and thus minimize the DNA extension. This constraint is removed in the high-flow zero-magnet cases (*). By selecting a "best fit" latitude for each bead, the force versus extension data from all points on the ellipse converge to one continuous curve, characteristic of the polymer.

Table 1. Persistence length values as a function of salt concentration.

$[Na^+]$ (mM)	a_{app} (Å)	a_{dyn} (Å)	a_{sta} (Å)
10	500*	700†	1750‡
1.0	675§	1100†	1750
0.1	1300§	4000†	1750

*Average obtained from bulk measurements (*1*). †Obtained by fitting the data to a contour length of 26 μm. ‡Calculated from a_{app} and a_{dyn} at 10 mM Na^+ with Eq. 5. This value is assumed to be salt-independent. §Calculated with Eq. 5.

ing magnetic beads are shown in Fig. 2A. Normally, the DNA was not stained and the molecular extensions were inferred from the positions of the bead as seen in transmission under dim light.

To determine the tension in the molecule for each bead position, the maximum magnetic force, F_M, acting on the bead was needed. Because the magnetic susceptibility varied considerably among beads, F_M had to be separately determined for each bead. Therefore, after the ellipse was generated, each bead was unleashed from its DNA tether and its velocity measured when acted upon by the maximum magnetic force. The value of F_M was determined with the well-known Stokes' relation (*15*):

$$F_M = 6\pi\eta r v \qquad (3)$$

where r is the bead's radius (*16*), η the buffer viscosity, and v was the bead's measured velocity through the stationary buffer. Knowing the magnetic force, the resultant of the magnetic and hydrodynamic forces acting on the bead and on the molecule (*17*) at each position was determined by angle θ in Fig. 1B.

Application of Stokes' law is justified by the Reynolds numbers in this experiment ($\sim 10^{-3}$). However, beads moving close to the glass surfaces experience increased viscous drag, which was manifested as poor velocity repeatability. Experiments were done in which the bead was timed while flying it halfway between the surfaces for various separations. These results (Fig. 2B) were compared to an expression derived by Lorentz (*18*) that corrects Stokes' law for a sphere moving parallel to a flat wetted surface:

$$F_M = 6\pi\eta r v\left(1 + \frac{9r}{16d}\right) \qquad (4)$$

where d is the distance from the center of the bead to the wall. Good repeatability was obtained by flying the bead halfway between the slide and cover slip in microchambers ~80 μm deep, where the correction is only 4%.

Typical force versus extension plots are shown in Fig. 3 for λ-dimers in 10 mM Na^+. For comparison, the predictions of the FJC model are plotted as continuous curves for three different Kuhn lengths and a contour length of 32.7 μm (Fig. 3A). At low extensions (inset, Fig. 3A), the data approach the middle curve, corresponding to a persistence length of 500 Å. However, the force required to further extend the molecules rises faster than predicted by the FJC model. The data appear to "cut the corner," rejoining the theoretical curves at forces greater than 10 pN.

The FJC model may fail because of its coarse description of DNA in terms of discrete segments. Perhaps the WLC model applied to force versus extension could account for the data but, to our knowledge, such a treatment is not available. Alternatively, the FJC and WLC models may both fail because they assume inextensibility of the molecule and ignore the possibility that DNA deforms under stress. Deformation would give rise to an enthalpic as well as an entropic component to the elasticity. The additional work done to extend the molecule, equal to the area between the data and the FJC curve, is then the enthalpy change of the molecule. Such enthalpic component could be associated with permanent small bends or local curvature of the DNA axis (*19*). Sequence-dependent bends are known to reduce the persistence length of the molecule (*20*, *21*), which would increase the molecule's contractibility.

The data might be better fit by an extensible FJC. A first model could involve a modified FJC constructed from a fixed number of bent segments whose length increase upon stress. At low forces, most of the work done on the chain would go toward orienting these segments' end-end vectors (decreasing entropy), whereas at higher forces additional work would be required to straighten the bends (increasing enthalpy).

A second model could involve a modified FJC made up of constant length (straight) segments whose number increases with stress. This chain would behave, at low stress, as if it had a shorter contour length (fewer Kuhn segments), but its elastic properties would be those of an ideal FJC chain possessing no bends or curvature. By choosing a shorter contour length, the data can be fit to FJC curves and we can estimate the value of the persistence length DNA should have would it not possess bends or curvature. Indeed, the low-force data (inset, Fig. 3B) is best fit by a FJC curve for a contour length of 26 μm and a persistence length

value of 700 Å (b = 0.14 μm), whereas the high-force data approaches the nominal contour length of 32.7 μm. The lowest number of segments is used for the FJC curve (inset, Fig. 3B) (N = 26/0.14 = 186) because the low-stress data corresponds to only 1% of the force required to completely extend the molecule, where N = 32.7/0.14 = 234.

The value of 700 Å is the persistence length of a molecule having no bends or curvature and has been called by Trifonov *et al.* (*20*) the "dynamic persistence length," a_{dyn}. Accordingly, the typical value of 500 Å determined in bulk measurements (*1*) corresponds to an "apparent persistence length," a_{app}, containing contributions from the dynamic and the "static persistence length," a_{sta}, associated with permanent local curvature (*22*). Because

$$1/a_{app} = 1/a_{dyn} + 1/a_{sta} \quad (5)$$

(*20*), this analysis yields a_{sta} = 1750 Å.

In Fig. 4A, semilogarithmic plots of force versus extension for individual molecules in three different ionic strengths are compared, illustrating the electrostatic contribution to DNA stiffness. At lower ionic strengths, the molecule becomes less contractile and therefore stiffer according to the FJC model. The data do not follow any particular FJC curve obtained with a 32.7-μm contour length. Instead, they span several FJC curves, making it difficult to assign unique persistence lengths at low-salt concentrations. If the FJC curves are redrawn with a contour length of 26 μm (Fig. 4B), the data conform more closely to FJC curves and values of dynamic persistence length can be estimated for the three ionic strengths, (Table 1).

These results assume invariance of the static persistence length, a reasonable albeit untested hypothesis. The apparent persistence lengths obtained in this way are well within the range of values determined by bulk methods (*23*). The dynamic persistence length is more sensitive to the ionic strength than the apparent value measured

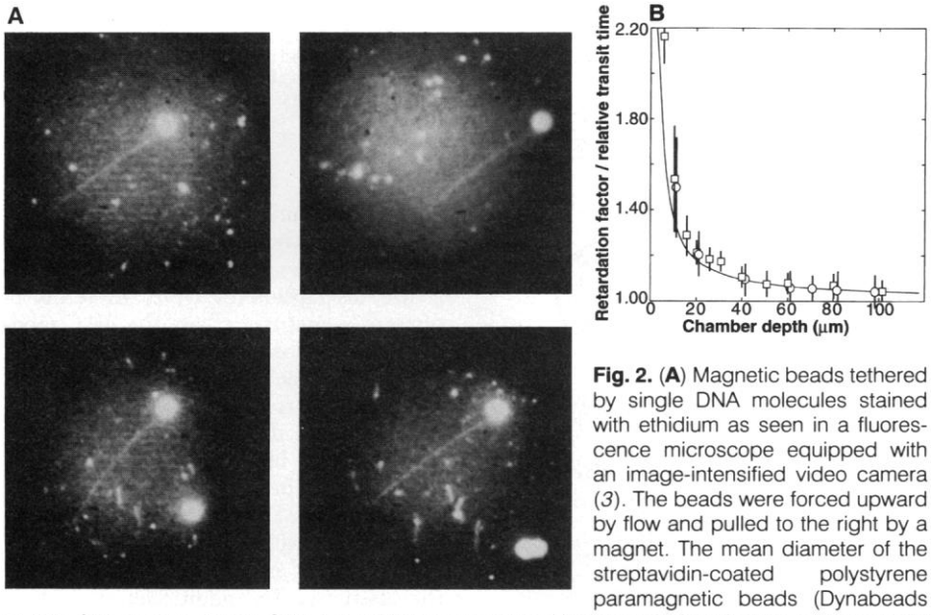

Fig. 2. (**A**) Magnetic beads tethered by single DNA molecules stained with ethidium as seen in a fluorescence microscope equipped with an image-intensified video camera (*3*). The beads were forced upward by flow and pulled to the right by a magnet. The mean diameter of the streptavidin-coated polystyrene paramagnetic beads (Dynabeads M-280, Streptavidin, Dynal, Oslo, Norway) was determined by transmission electron microscopy to be 2.9 μm with a 3% coefficient of variation (cv, standard deviation/mean). Magnetic susceptibilities of the beads were less uniform (cv = 33%) as determined with Stokes' law. With our magnets, F_M values ranged between 0.4 and 2 pN. (**B**) The transit times of a single bead were measured as it was repeatedly pulled back and forth across a 70-μm space by the maximum magnetic force F_M. The bead was levitated halfway between slide and cover slip. Each data point represents 10 to 20 transit times with the vertical bar being the standard deviation in those times. The depth of the chamber was adjusted by changing its internal pressure. Circles and squares represent two different beads. The continuous line is the correction factor of Eq. 4, but with its second term doubled to account for the presence of two surfaces instead of one. The transit times were normalized to agree exactly with the continuous line at the largest chamber depth used.

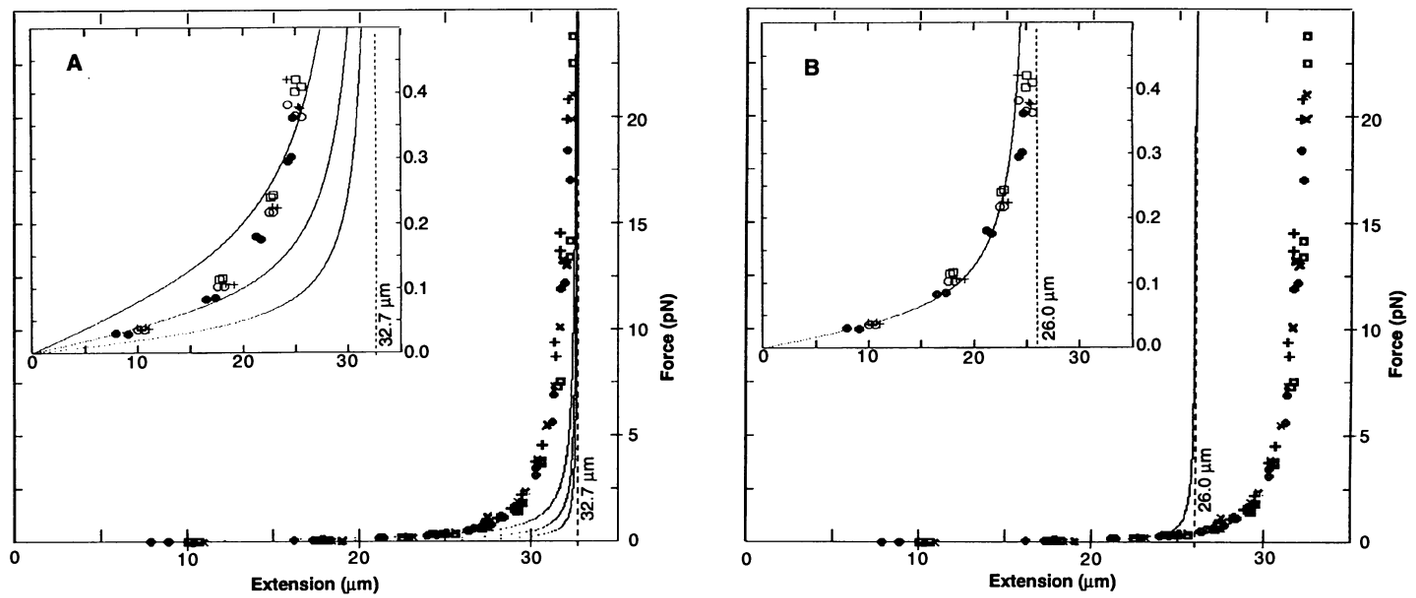

Fig. 3. (**A**) Force versus extension data for four different λ-dimer molecules (●, □, +, and ○) in 5 mM Na_2HPO_4 buffer (10 mM Na^+, pH 8.3). Inset: expanded vertical scale (0 to 0.5 pN). Continuous curves are from Eq. 2 assuming L = 32.7 μm and b = 500 Å (top), 1000 Å (middle), and 2000 Å (lower). L = 32.7 μm was chosen to agree with the accepted value of 3.37 Å rise per base pair (*30*), not to fit the data. (**B**) The same data compared with a Langevin curve L = 26 μm and b = 1400 Å. These values were chosen to match the low-force slope.

in bulk experiments, a consequence of the finite value of the static persistence length in naturally occurring DNA.

The effect of ethidium bromide on the force curves is shown in Fig. 5A. As the molecule is exposed to higher dye concentrations, its contour length increases until a maximum elongation of ~40% is attained, in agreement with other estimates (*24*). Surprisingly, the elasticity of the molecule is not altered by ethidium intercalation, suggesting that the dye changes neither the short-range nor the long-range (electrostatic) components of the bending rigidity. To within the sensitivity of the method, the fully intercalated molecules behave as uncomplexed molecules that are 40% longer (*25*). A similar result is observed for λ molecules complexed with 4′,6-diamidino-2-phenylindole (DAPI). Extensions of 10 and 17% were observed at DAPI concentrations of 0.05 and 0.5 μg/ml, respectively, in 10 mM Na^+, with force curves similar to those of ethidium. DAPI exhibits various modes of interaction, including minor groove binding, and preferential intercalation next to GC base pairs (*26*). The elongation value of 17% obtained here strongly confirms the existence of an intercalative mode but indicates fewer binding sites than the usual intercalator, in agreement with hydrodynamic and spectroscopic studies (*27*).

Apparent binding constants for ethidium ($3.9 \times 10^6\ M^{-1}$) and for DAPI ($8.0 \times 10^6\ M^{-1}$) in 10 mM Na^+ are readily obtained as the inverse of the dye concentrations required to lengthen the molecule by one-half of the maximum elongation observed (40%).

The elastic response of three molecules pretreated with *cis*-diamminedichloroplatinum (II) (DDP), which introduces local bends in DNA by cross-linking adjacent adenines (*28*), is shown in Fig. 5B. DDP incorporation did not always show the expected stoichiometric yield, but the number of bends introduced can be estimated indirectly. One treated molecule from Fig. 5B, upon exposure to ethidium bromide, lengthened only 30% instead of the usual 40%. Presumably one-fourth of the possible intercalation sites had been excluded by cross-linking, as described in other studies (*29*). These molecules are more contractile than natural DNA at all extensions, probably because of the extra work required to straighten the artificial bends. The maximum extension is the same as for untreated DNA, suggesting that high forces completely straighten the bends. The observed "corner cutting" is more pronounced than in natural DNA, supporting the hypothesis that bends in natural DNA cause its deviation from FJC theory.

The low-force data approach the upper FJC curve indicating that $a_{app} = 250$ Å. If we assume that $a_{dyn} = 700$ Å, as in natural DNA at 10 mM Na^+, then $a_{sta} = 390$ Å. Indeed, the data conform to the 700 Å FJC curve if treated as in Fig. 3B with the contour length reduced 40% to 20 μm. This analysis is supported by electron micrographs of DDP-treated molecules that show an apparent 40% contour length reduction under similar conditions (*29*).

These results illustrate the limitations of the simple FJC theory to describe the force versus extension data of DNA molecules. It has not been our intention here to present an alternative theoretical model but to suggest a line of reasoning that supports the interpretation of the data in terms of sequence-dependent permanent bends in naturally occurring DNA. Better theoretical models incorporating the rapidly growing knowledge on sequence dependence curvature in DNA (*21*) will be necessary. Similar experiments carried out on chromatin may provide insight on how the elastic properties of DNA are modified by its interaction with histones. If a tethered DNA molecule can be prevented from swiveling at its points of attachment, then the permanent magnetic dipole of the bead can be used, along with a rotating magnetic field, to spin the bead and supercoil the molecule. Comparison of force versus extension curves of supercoiled molecules to those obtained here, should make it possible to determine the energy of supercoiling of DNA and its torsional rigidity.

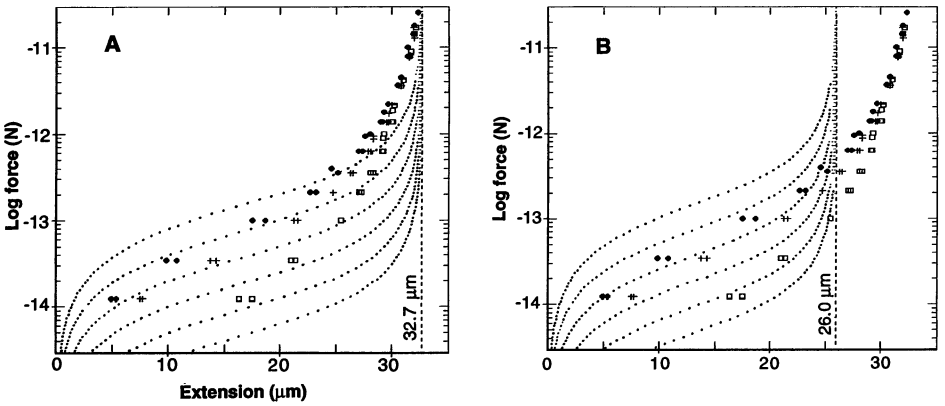

Fig. 4. (**A**) Semilogarithmic plot of force versus extension for a single λ-dimer molecule in three different Na^+ concentrations (from Na_2HPO_4): [Na^+] = 10^{-2} M (●); 10^{-3} M (+); and 10^{-4} M (□). The dotted curves are from Eq. 2 for L = 32.7 mm, b = 500 Å (top), and 1,000, 2,000, 4,000, 8,000, and 16,000 Å (bottom). (**B**) The same data compared with Eq. 2 force curves where L = 26 μm.

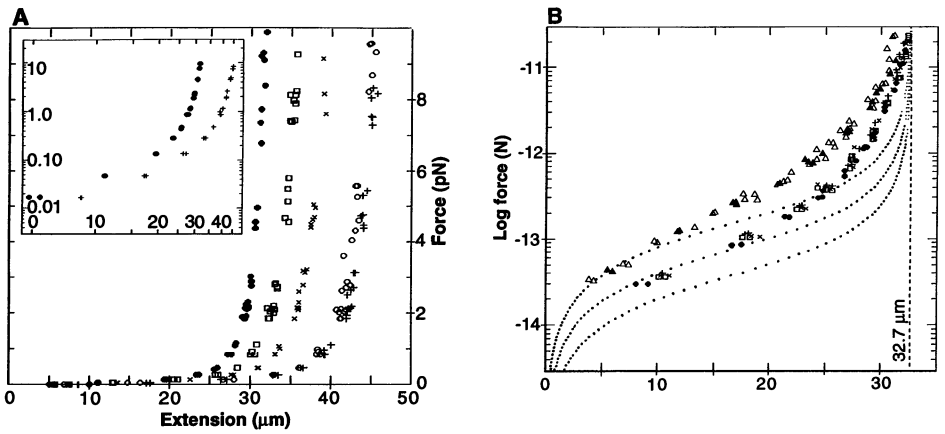

Fig. 5. (**A**) Force curves of a λ-dimer in 5 mM Na_2HPO_4 with various concentrations of ethidium bromide (Aldrich): (●) unstained; (□) 0.03 μg/ml; (×) 0.10 μg/ml; (○) 1.0 μg/ml; and (+) 2.0 μg/ml. If the intrinsic elastic properties of DNA do not change with intercalation, but molecules simply become longer by some factor, then the extensions would be increased by the same factor for all forces in the curve. In a log-log plot (see inset), the curve of the stained molecule would reproduce the curve of the native molecule but would be shifted to the right. Indeed, the curves are quite parallel except at the lowest forces where they diverge somewhat, perhaps because of an increasing persistence length with intercalation. The divergence, however, is close to the low-extension repeatability error of ±1 μm. (**B**) Four native λ-dimers (●, □, ×, and +; same data as in Fig. 3), compared with three DDP-treated DNA molecules. Two of these are λ-monomers (△), shown double length for comparison, and one is a λ-dimer (▲). The DNA (concentration 400 ng/ml) and DDP (100 ng/ml) were reacted in 10 mM $NaClO_4$ buffer, in darkness, at 37°C for 24 hours.

REFERENCES AND NOTES

1. P. J. Hagerman, *Annu. Rev. Biophys. Biophys. Chem.* **17**, 265 (1988).
2. M. Yanagida, Y. Hiraoka, I. Katsura, *Cold Spring Harbor Symp. Quant. Biol.* **47**, 177 (1983).
3. T. W. Houseal, C. Bustamante, R. F. Stump, M. F. Maestre, *Biophys. J.* **56**, 507 (1989).
4. S. B. Smith, P. K. Aldridge, J. B. Callis, *Science* **243**, 203 (1989).
5. D. C. Schwartz and M. Koval, *Nature* **338**, 520 (1989).
6. C. Bustamante, *Annu. Rev. Biophys. Biophys. Chem.* **20**, 415 (1991).
7. Single DNA molecule elasticity have been previously estimated by other authors (*2, 3*) using various ways of stretching, including optical tweezers [M. Kasevich *et al.*, *Proceedings of the Twelfth International Conference on Atomic Physics*, J. C. Zorn and R. R. Lewis, Eds. (American Institute of Physics, New York, 1990), pp. 53–57; S. Chu, *Science* **253**, 861 (1991)]. However, all of these methods measure the rate of contraction of a stretched molecule and require an estimation of the DNA drag coefficient. The static experiments presented here avoid this requirement.
8. B. H. Zimm and S. D. Levene, *Q. Rev. Biophys.*, in press.
9. B. Åkerman, M. Jonsson, B. Norden, *Biopolymers* **28**, 1541 (1989).
10. D. Stigter, *ibid.* **31**, 169 (1991).
11. F. Bueche, *Physical Properties of Polymers* (Interscience, New York, 1962), p. 37. No account is made in the derivation of Eq. 1 for the volume excluded from the polymer by the glass surface. However, although the presence of the wall reduces the number of accessible configurations to the chain [see E. F. Cassasa, *Polym. Lett.* **5**, 773 (1967); E. A. Di Marzio, *J. Chem. Phys.* **42**, 2101 (1965)], the tension in the chain, which is proportional to the gradient of its configurational entropy, is not affected in directions parallel to the plane of the wall, along which the chain is pulled.
12. P. J. Flory, *Statistical Mechanics of Chain Molecules* (Hanser, Munich, 1989), pp. 307–338 and 401.
13. Ligated 97-kbp dimers of methylated phage λ DNA, strain c1857ind1 Sam 7 (NEB) were used. The left sticky end of the dimer is hybridized and ligated to a 12-base oligo, 3′ end-labeled previously with digoxigenin (Boehringer Genius-5). The right sticky end is similarly attached to a 12-base oligo constructed with a 3′ biotin end-label (Glenn Research). The glass microscope slide is successively coated with γ-aminopropyltriethoxysilane (Pierce), protein A, polyclonal antidigoxigenin (Boehringer), and finally cross-linked with dimethyl pimelimidate (Pierce). The molecule ends were labeled differently to prevent attachment of both ends of the DNA to either the glass or the bead. The DNA is free to swivel about either point of attachment.
14. All equilibrium bead positions are time averages over the Brownian motion. Error is incurred when the position is averaged for a limited time with low-force points requiring longer times. For forces below 30 fN, averaging times >5 min yield errors of ±1 μm. High-force extensions can be measured in a few seconds to within ±0.3 μm.
15. C. R. Cantor and P. R. Schimmel, *Biophysical Chemistry Part II* (Freeman, New York, 1980), pp. 557–558.
16. The radius of a particular bead is checked through the optical microscope to within ±3%, leading to 3% uncertainty in the force, in addition to possible systematic error in the hydrodynamic radius. The viscous drag coefficient was checked by observing beads of known density fall through water. Equating the underwater weight with the Stokes' law drag gave a hydrodynamic radius 6% greater than the observed mechanical radius of 2.9 μm. This difference could be due to surface roughness or it could be an error in our estimate of the bead's volume due to porosities. The mechanical radius was used in all of the experiments shown here.
17. Close examination of Fig. 2A shows the molecules are curved because of hydrodynamic drag of DNA, which can be determined with only the curve shape and the bead radius, assuming a homogeneous flow field. The drag coefficient for a λ-dimer obtained is roughly one-half of that of a 2.9-μm bead. As a result, the tension next to the slide end of the molecule exceeds that at the bead end by as much as 50% in high flows. The tension that is measured by the angle method (caption to Fig. 1B) and plotted as force data is the average tension in the molecule. The curvature of DNA in Fig. 2A increases its path length only a negligible amount.
18. H. A. Lorentz, *Abhandlungen über Theoretische Physik* (Teubner, Leipzig, 1907), pp. 23–42.
19. Only one region of λ-DNA is highly bent, as shown by the anomalous gel mobility it confers to restriction fragments [see K. Zahn and F. R. Blattner, *Nature* **317**, 451 (1985)]. This region is unlikely to account for these results by itself, however, DNA curvature associated with random sequences could be both appreciable and ubiquitous (*21, 22*).
20. E. N. Trifonov, R. K.-Z. Tan, S. C. Harvey, in *Structure and Expression*, vol. 3: *DNA Bending and Curvature*, W. K. Olson, R. H. Sarma, M. Sundaralingam, Eds. (Adenine, New York, 1987), pp. 243–253.
21. A. Bolshoy, P. McNamara, R. E. Harrington, E. N. Trifonov, *Proc. Natl. Acad. Sci. U.S.A.* **88**, 2312 (1991).
22. Persistence length is a measure of the tendency of a chain to persist in some initial direction. Deflections from this direction can be caused by either thermal fluctuations or permanent bends. An inherently straight molecule at finite temperature would display a purely dynamic persistence length due to thermal fluctuations. An inherently bent molecule would display only its static persistence length at 0 K and an apparent persistence length at finite temperature.
23. P. J. Hagerman, *Biopolymers* **20**, 1503 (1981); E. S. Sobel and J. A. Harpst, *ibid.* **31**, 1559 (1991).
24. H. J. Vollenweider, A. James, W. Szybalski, *Biochemistry* **75**, 710 (1978).
25. The ethidium insensitivity of the "corner cutting" in the force curves is somewhat surprising. We can only list here the possible explanations: (i) ethidium does not bind to the bent regions in DNA; (ii) ethidium binds to bent regions but it does not change the local curvature; (iii) ethidium undoes the curvature of the bent regions but induces new curvature in inherently straight locations leading to a compensation effect; and (iv) corner cutting is not caused by bent regions. The latter is less likely as shown by the DDP experiments further in the text.
26. W. D. Wilson *et al.*, *Biochemistry* **29**, 8452 (1990).
27. G. Manzini, M. L. Barcellona, M. Avitabile, F. Quadrifoglio, *Nucleic Acids Res.* **11**, 8861 (1983).
28. N. P. Johnson *et al.*, in *Progress in Clinical Biochemistry and Medicine* (Springer-Verlag, Berlin, 1989), vol. 10, pp. 1–24.
29. J.-P. Macquet and J.-L. Butour, *Biochemie* **60**, 901 (1978).
30. W. Saenger, *Principles of Nucleic Acid Structure* (Springer-Verlag, New York, 1984), p. 226.

31. We thank J. Schellman, H. Reese, N. Johnson, and P. Sebring for many useful discussions. Supported by National Institutes of Health grant GM 32543 and National Science Foundation MCB 9118482 to C.B. Additional Funding was provided by the Lucille P. Markey Charitable Trust.

17 July 1992; accepted 10 September 1992

Complete Wetting from Polymer Mixtures

Ullrich Steiner, Jacob Klein,* Erika Eiser, Andrzej Budkowski,† Lewis J. Fetters

Coexisting polymer phases are characterized by very small interfacial energies, even well below their critical solution temperature. This situation should readily lead to the exclusion of one of the phases from any interface that favors the other. Such complete wetting behavior from a binary mixture of statistical olefinic copolymers is reported. By means of a self-regulating geometry, it is found that the thickness of a wetting layer of one of the phases at the polymer-air interface, growing from the other coexisting phase, attains macroscopic dimensions, increasing logarithmically with time. These results indicate that binary polymer mixtures could be attractive models for the study of wetting phenomena.

A surface in contact with a mixture of two fluid phases will generally favor one of them. The surface may be partially wetted, in which case it will be covered by a microscopic layer of the favored phase, or it may be covered by a thick, macroscopic layer of this phase for the case of complete wetting (*1*). This transition between partial and complete wetting is implicit in the early work of Young (and of Laplace) on the contact angle of liquid drops on a surface (*2*), but it is only recently that the physics of such transitions has come into sharper focus. In a seminal paper (*3*), Cahn in 1977 proposed that a transition from partial to complete wetting from a binary mixture must always occur when the temperature T is raised sufficiently close to the upper critical solution temperature T_c (the highest temperature at which two phases can coexist) of the mixture. In the ensuing years, there have been extensive theoretical and experimental studies of such transitions (*4, 5*). Among the outstanding unresolved issues is that of wetting from macromolecular mixtures (*6, 7*). In these mixtures, complete wetting is predicted to occur readily, and far from T_c (*7*); yet such wetting has

U. Steiner, J. Klein, E. Eiser, A. Budkowski, Department of Materials and Interfaces, Weizmann Institute of Science, Rehovot 76100, Israel.
L. J. Fetters, Exxon Research and Engineering Corporation, Annandale, NJ 08801.

*To whom correspondence should be addressed.
†On leave from Jagellonian University, Cracow, Poland.